"A Dynamic Wideband Directional Channel Model for Vehicle-to-Vehicle Communications"

He, Ruisi ; Renaudin, Olivier ; Kolmonen, Veli-Matti ; Haneda, Katsuyuki ; Zhong, Zhangdui ; Ai, Bo ; Oestges, Claude

Abstract

Vehicle-to-vehicle (V2V) communications have received a lot of attention due to their numerous applications in traffic safety. The design, testing, and improvement of the V2V system hinge critically on the understanding of the propagation channels. An important feature of the V2V channel is the time variance. To statistically model the time-variant V2V channels, a dynamic wideband directional channel model is proposed in this paper, based on measurements conducted at 5.3 GHz in suburban, urban, and underground parking environments. The model incorporates both angular and delay domain properties and the dynamic evolution of multipath components (MPCs). The correlation matrix distance is used to determine the size of local wide-sense stationary (WSS) region. Within each WSS time window, MPCs are extracted using the Bartlett beamformer. A multipath distance-based tracking algorithm is used to identify the “birth” and “death” of such paths over different stationarity regions, and...

Document type : *Article de périodique (Journal article)*

This article has been accepted for publication in a future issue of this journal, but has not been fully edited. Content may change prior to final publication. Citation information: DOI 10.1109/TIE.2015.2459376, IEEE Transactions on Industrial Electronics

A Dynamic Wideband Directional Channel Model for Vehicle-to-Vehicle Communications

Ruisi He, *Member, IEEE*, Olivier Renaudin, Veli-Matti Kolmonen, Katsuyuki Haneda, *Member, IEEE*, Zhangdui Zhong, Bo Ai, *Senior Member, IEEE*, and Claude Oestges, *Senior Member, IEEE*

***Abstract*—Vehicle-to-vehicle (V2V) communications have received a lot of attention due to its numerous applications in traffic safety. The design, testing, and improvement of the V2V system hinges critically on the understanding of the propagation channels. An important feature of the V2V channel is the time-variance. To statistically model the time-variant V2V channels, a dynamic wideband directional channel model is proposed in this paper, based on measurements conducted at 5.3 GHz in suburban, urban, and underground parking environments. The model incorporates both angular and delay domain properties as well as the dynamic evolution of multipath components (MPCs). The correlation matrix distance is used to determine the size of local wide-sense stationary (WSS) region. Within each WSS time window, MPCs are extracted using the Bartlett beamformer. A multipath distance-based tracking algorithm is used to identify the "birth" and "death" of such paths over different stationarity regions, and the lifetime of MPC is modeled with a truncated Gaussian distribution. Distributions for the number of multipaths and their positions are statistically modeled. Within each path lifetime, the initial power is found to depend on the excess delay, and a linear polynomial function is used to model the variations within the lifetime. In addition, a Nakagami distribution is suggested to describe the fading behavior. Finally, the model implementation is validated by comparison of second-order statistics between measurements and simulations.**

***Index Terms*—Antenna arrays, dynamic model, MPC lifetime, MPC tracking, propagation, vehicle-to-vehicle communications.**

I. Introduction

CHANNEL modeling has been an important research topic in wireless communications, since the performance of any practical system is determined by the channel. In general, wireless channels are time variant, which gives rise to considerable theoretical challenges to channel characterization. Fortunately, most wireless channels can be classified as wide-sense stationary (WSS) [2]. However, practical channels never exactly satisfy the WSS assumption due to the motions of transmitter (Tx) and receiver (Rx), and changes of surrounding scatterers. Especially in those environments with a large number of dynamic scatterers, as is the case for vehicle-to-vehicle (V2V) channels, this time-variant behavior should be carefully incorporated in channel modeling.

V2V channel modeling has gained much interest in the last few years because of the potential applications in the Intelligent Transportation Systems. The motions of Tx and Rx in V2V environments introduce both small- and large-scale variations in the received signal, and thus results in time-variant channels. Since deterministic simulations usually require a large computational effort, creating an exact dynamic environments to incorporate time-variant behavior is not feasible [3]. Therefore, statistical models, which have the advantage of reduced simulation times, have been widely adopted. Even though many statistical channel models have been developed for V2V communications [4]–[6], most papers do not model the dynamic variations of multipath statistics over different WSS regions. A static channel model with constant parameter settings is insufficient to realistically model the time-variant V2V channels, and [7] shows that the assumption of WSS leads to (erroneous) optimistic bit error rate in single-carrier and multi-carrier system simulations. Currently, there lacks detailed characterization of dynamic channel parameters such as fluctuations of the number of multipath components (MPCs), lifetimes of MPCs, appearance and disappearance behaviors of MPCs, etc. Even though some recent papers have investigated the time-variant V2V channels, those papers either focus on the characterization of the size of local WSS region and do not present the dynamic channel modeling [8], [9], or consider the channel statistics of MPC to be constant within the lifetime and do not analyze the angular domain variations [10], [11]. To the best of the authors' knowledge, the complete *dynamic behaviors* of MPCs, have not been well characterized in V2V environments.

The literature on dynamic channel models, that is, channel models with time-varying parameters, is relatively scarce, and is mostly for non-V2V environments. In [12], a dynamic indoor directional-channel simulator is proposed using a two-

Manuscript received November 8, 2014; revised June 5, 2015 and June 20, 2015; accepted June 21, 2015.

Part of the work is presented in the IEEE VTC-Spring 2015 [1].

This work was supported by China Postdoctoral Science Foundation under Grant 2015M570030, the State Key Laboratory of Rail Traffic Control and Safety under Grant RCS2015ZQ003, the Fundamental Research Funds for the Central Universities under Grant 2015RC025, the Key Grant Project of Chinese Ministry of Education (No.313006), the National Natural Science Foundation of China under Grant 61222105 and U1334202, and the National 863 Project under Grant 2014AA01A706. (*Corresponding author: B. Ai.*)

R. He, Z. Zhong, and B. Ai are with the State Key Laboratory of Rail Traffic Control and Safety, Beijing Jiaotong University, Beijing 100044, China (e-mail: ruisi.he@bjtu.edu.cn, zhdzhong@bjtu.edu.cn, boai@bjtu.edu.cn).

O. Renaudin is with the Department of Electrical and Engineering, University of Southern California, Los Angeles, USA (e-mail: renaudin@usc.edu).

V.-M. Kolmonen is with Nokia Technologies, Finland (e-mail: velimatti.kolmonen@iki.fi).

K. Haneda is with the Department of Radio Science and Engineering, Aalto University, Aalto 00076, Finland (e-mail: katsuyuki.haneda@aalto.fi).

C. Oestges is with the Institute for Information and Communication Technologies, Electronics and Applied Mathematics, Université Catholique de Louvain, 1348 Louvain-la-Neuve, Belgium (e-mail: claude.oestges@uclouvain.be).

This article has been accepted for publication in a future issue of this journal, but has not been fully edited. Content may change prior to final publication. Citation information: DOI 10.1109/TIE.2015.2459376, IEEE Transactions on Industrial Electronics

state semi-Markov model. In [13], a measurement-based dynamic indoor channel model is proposed based on a 4-state Markov process. In [14], a dynamic temporal domain model is proposed in indoor environment. In [15], a geometrically-based statistical model is proposed and dynamic behaviors of MPCs are modeled. In [16], a time-variant channel model, combined with the geometry-based stochastic model, is proposed for indoor positioning. In [17], [18], the theory of spatial point processes is employed to analytically describe birth-death dynamics of time-variant radio channels. Above overview shows that the dynamic channel modeling has been mostly performed in indoor environments. Compared with the V2V channels, the indoor channels have fewer dynamic scatterers, which makes it easier to track the dynamic variations of MPCs [19]. While these works might not be readily scalable to V2V environments, they provide some insight into dynamic channel modeling.

In our previous work [1], the dynamic behaviors of MPCs are briefly analyzed. In this paper, we propose an empirical dynamic V2V model, which characterizes angular and delay properties as well as dynamic evolution of MPCs as the Tx and Rx move. The number of MPCs, lifetimes, positions (delay and angle), and dynamic variations within their lifetimes are statistically modeled. The proposed model shows insight into the dynamic behaviors of MPCs in V2V environments, which improves the understanding of time-variant V2V channels, and provides a more realistic simulation model for performance evaluation.

The remainder of the paper is organized as follows. Section II proposes the dynamic channel model. Section III introduces measurement campaign for the model parameterization. Section IV describes data processing techniques to extract and track MPCs. Section V shows the model parameters. Section VI presents model implementation and validation. Finally, Section VII concludes the paper.

II. Dynamic Channel Model

To incorporates the time-variant characteristics of V2V channels, we propose a new dynamic tapped-delay-angle-line model in this section. The directional channel impulse response can be expressed as

$$h(t_i,\tau_l(t_i),\phi_l(t_i)) = \sum_{l=1}^{N(t_i)} a_l(t_i)e^{j\varphi_l}\cdot\delta\left(\tau-\tau_l(t_i)\right)\cdot\delta\left(\phi-\phi_l(t_i)\right), \quad (1)$$

where $\delta(\cdot)$ is the Dirac delta function; $N(t_i)$ is number of MPCs; $a_l(t_i)$, $\tau_l(t_i)$, and $\phi_l(t_i)$ are amplitude, delay, and angle[1] of the lth MPC at time t_i. In (1), $N(t_i)$, $a_l(t_i)$, $\tau_l(t_i)$, and $\phi_l(t_i)$ are time-variant; φ_l is the phase and is assumed to be uniformly distributed over the range of $[0,360]^\circ$.

For the time-variant V2V channels, the behavior of each MPC changes over time. Owing to Rx and Tx motion as well as dynamic scatterers, each MPC could randomly appear at a certain time instant and vanish at another time instant; and within its lifetime, the amplitude, delay, and angle are all time-variant. For convenience, we define three sets of MPCs in (1):

- $\mathcal{L}_{i\to i}$ is the set of MPCs that are firstly observed at time t_i, whose index of path is $l_{i\to i}=1,2,\cdots,N(t_{i\to i})$.
- $\mathcal{L}_{j\to i}$ is the set of MPCs that are firstly observed at time t_j (where $0<j<i$) and still exist at time t_i, whose index of path is $l_{j\to i}=1,2,\cdots,N(t_{j\to i})$.
- $\mathcal{L}_i$ is the set of all the MPCs that exist at time t_i, i.e., $\mathcal{L}_i=\mathcal{L}_{1\to i}\cup\mathcal{L}_{2\to i}\cup\cdots\mathcal{L}_{j\to i}\cup\cdots\mathcal{L}_{i-1\to i}\cup\mathcal{L}_{i\to i}$.

By identifying and tracking MPCs in all sets of $\mathcal{L}_{i\to i}$ and $\mathcal{L}_{j\to i}$, the directional channel impulse response at time t_i can be reconstructed, and the time-variant characteristics are automatically incorporated. Eq. (1) can thus be expressed as

$$\begin{aligned} h(t_i,\tau(t_i),\phi(t_i)) = & \sum_{j=1}^{i-1}\sum_{l_{j\to i}=1}^{N(t_{j\to i})}\left[a_{l_{j\to i}}(t_i)e^{j\varphi_{l_{j\to i}}}\right. \\ & \left.\cdot\,\delta\left(\tau-\tau_{l_{j\to i}}(t_i)\right)\cdot\delta\left(\phi-\phi_{l_{j\to i}}(t_i)\right)\right] \quad , \quad (2) \\ + & \sum_{l_{i\to i}=1}^{N(t_{i\to i})}\left[a_{l_{i\to i}}(t_i)e^{j\varphi_{l_{i\to i}}}\right. \\ & \left.\cdot\,\delta\left(\tau-\tau_{l_{i\to i}}(t_i)\right)\cdot\delta\left(\phi-\phi_{l_{i\to i}}(t_i)\right)\right] \end{aligned}$$

where

$$N(t_i)=N(t_{i\to i})+\sum_{j=1}^{i-1}N(t_{j\to i}). \quad (3)$$

The first term on the right side of Eq. (2) represents the MPCs that have been observed before time t_i, i.e., *old* MPCs[2]; and the second term of Eq. (2) represents the MPCs that are firstly observed at time t_i, i.e., *new* MPCs. The approach of the dynamic channel modeling is to incorporate the "birth" and "death" evolutions of MPCs at any time instant. By modeling the dynamic evolutions of new and old MPCs, respectively, the model can generate the dynamic impulse response at any time. Note that we ignore the cases where MPCs re-appear after they have vanished. When a MPC vanishes, its lifetime ends. This assumption simplifies the channel modeling and does not significantly affect the model accuracy [20].

For time-variant V2V channels, parameters in (1) and (2) are randomly time-varying functions. To statistically model them, a local WSS region (i.e., a WSS time window) $\Delta\overline{W}$ should be defined[3], so that the statistics of parameters can be characterized statistically within each WSS time window [21]–[23] and the channel modeling becomes physically meaningful. Note that based on the description of (2), MPC lifetime is usually larger than the size of $\Delta\overline{W}$, i.e., one MPC can exist in multiple consecutive WSS regions. Therefore, the MPC can be characterized in terms of how many WSS windows are spanned over its lifetime. This also implies that the dynamic evolution of each MPC over different WSS regions must be included in our channel modeling. To this end, we use two

[1]Here we only consider azimuth angle of arrival. The reason is presented in the next section.

[2]Note that the old MPCs can be further divided into two subcategories: (i) the MPCs whose lives continue into the following time instant; and (ii) the MPCs whose lives end in the particular time instant of t_i. By assigning an initial lifetime to each new MPC, the evolutions of above two subcategories of MPCs can be incorporated into the dynamic model.

[3]In this paper, the local WSS region means that the statistics of the channel within each WSS time window are similar enough so that the statistics can be approximately considered to be stationary.

This article has been accepted for publication in a future issue of this journal, but has not been fully edited. Content may change prior to final publication. Citation information: DOI 10.1109/TIE.2015.2459376, IEEE Transactions on Industrial Electronics

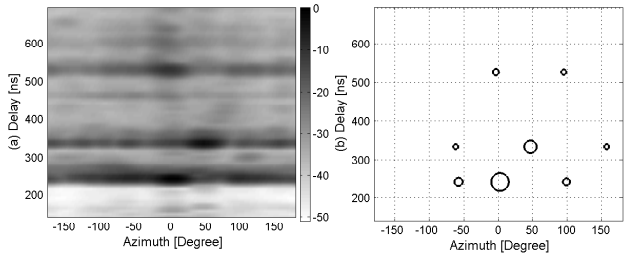

Fig. 1. Example results from suburban measurements. (a) AOA-delay spectrum in dB. (b) Detected MPCs. A larger size of the circle depicts a higher power carried by MPC.

distinct time scales to describe each MPC over its lifetime:

- large-scale variations: MPC average power, angle and delay are indexed by the WSS window index; this means that these values remain fixed within a WSS window and then change from one WSS window to the next one,
- small-scale variations: MPC instantaneous power follows a given fading distribution within each WSS window, whereas angle and delay remain fixed over small-scale durations.

To summarize, in the proposed model, we statistically model the following parameters:

- the size of MPC lifetime in terms of WSS windows,
- the number of the newly observed MPCs in each WSS time window,
- the initial power, angle and delay of the newly observed MPCs in each WSS time window,
- the dynamic evolution of power/delay/angle of each MPC over different WSS regions within the MPC lifetime,
- the MPC small-scale fading in each WSS time window.

With statistical models of the above parameters, a dynamic model can be developed to simulate time-variant channels.

III. Measurement

In this section, we describe the V2V measurement campaign that serves as the basis for the model parameterization. We only give a brief summary; detailed descriptions can be found in [24].

A. Measurement system

Measurements were conducted with the Aalto channel sounder [25] at 5.3 GHz and a bandwidth of 60 MHz, which is close to the 5.9 GHz V2V band. The difference between 5.3 GHz and 5.9 GHz is 11% (=0.6/5.3), so their propagation channel characteristics do not change much. Since we do not have measurements at the two frequencies in the considered V2V scenario, we cannot quantify the difference. However, other measurements using the ultrawideband signal show that the path loss exponent has a variation of less than 15% over 1 GHz bandwidth [26] and the delay spread has less than 10% variation over 8 GHz bandwidth [27]. We could regard these values as an uncertainty of the estimated model parameters at 5.3 GHz, when the goal is to estimate parameter values at 5.9 GHz. This is also the same assumption behind WINNER [28] and COST [29] standard models which can be used between 2 GHz and 6 GHz. The sampling frequency is 120 MHz and snapshot interval $t_{\mathrm{rep}} = 15$ ms. We used a dual-polarized semi-spherical antenna array at Rx side, which consists of 15 dual-polarized elements (i.e. 30 feeds). A Uniform Linear Array (ULA) with 4 vertically polarized antennas was used at Tx side. Therefore, the MIMO channel matrix is $N_{\mathrm{Rx}} \times N_{\mathrm{Tx}} = 30 \times 4$, where N_{Tx} and N_{Rx} are numbers of Tx and Rx antennas.

B. Environment

Measurements were conducted in three scenarios in Finland:

- Suburban: It consists of small detached houses and an average tree density of roughly 5 m high. Measurements were conduced in 14 different routes in suburban, with 63700 snapshots (i.e., MIMO channel matrices) in total.
- Urban: It is in the city center of Tapiola, Finland, which consists of three to four-storey buildings on both sides of two-lane streets. Measurements were conducted in 2 different routes in suburban, with 7700 snapshots in total.
- Underground parking: It is under the ground of Tapiola city center, with rich scatterers due to the tunnel-like structure. Measurements were conducted in 3 different routes in suburban, with 12000 snapshots in total.

Measurements were conducted with two compact cars (driving in the same direction) under line-of-sight (LOS) conditions.

IV. Data Processing

A. MPC Identification

To perform the above statistical channel modeling, the information of each MPC (e.g., a_l, τ_l, and ϕ_l) need to be extracted. In this paper, the Bartlett beamformer is used, which has reasonable accuracy and low computational complexity when using a large antenna array [30]. We only consider azimuth-of-arrival (AOA) domain because: i) the number of Tx antennas is small, which limits resolution of the analysis on azimuth-of-departure (AOD) domain; ii) in our scenarios, the distribution of scatterers does not change significantly on elevation domain[4]. The power-angular-delay-profile (PADP) (averaged over the s-th WSS time window[5]) of Bartlett beamformer is expressed as

$$P_h(t_s, \tau_s, \phi_s) = \boldsymbol{\alpha}^{\mathrm{H}}(\phi_s) \cdot \mathbf{R}(t_s, \tau_s) \cdot \boldsymbol{\alpha}(\phi_s) \ , \qquad (4)$$

[4]The estimated angle of elevation remains almost always around 90 degrees, i.e. in the horizontal plane (parallel to the ground surface).

[5]In this paper, i and j represent indices of instantaneous snapshots as in Eq. (1); whereas s in Eq. (4) represents index of WSS time windows.

This article has been accepted for publication in a future issue of this journal, but has not been fully edited. Content may change prior to final publication. Citation information: DOI 10.1109/TIE.2015.2459376, IEEE Transactions on Industrial Electronics

where $(\cdot)^{\mathrm{H}}$ denotes hermitian transpose; ϕ_s is angle of azimuth; $\boldsymbol{\alpha}(\phi_s)$ is the steering vector, which is defined as the projection of array manifold onto polarization direction of the incident signal [31], [32]. We only consider co-polarization case to better identify MPCs from spatial spectrum. Within the s-th WSS region, at time t_i, let us define $\mathbf{W}$ as

$$\mathbf{W}(t_i,\tau_i) = \frac{1}{(N_{\mathrm{Tx}})^2}\left(\sum_{n_{\mathrm{T}}=1}^{N_{\mathrm{Tx}}}\mathbf{h}(n_{\mathrm{T}},t_i,\tau_i)\right)\left(\sum_{n_{\mathrm{T}}=1}^{N_{\mathrm{Tx}}}\mathbf{h}(n_{\mathrm{T}},t_i,\tau_i)\right)^{\mathrm{H}}, \tag{5}$$

where time t_i is within the s-th WSS time window, and $\mathbf{h}(n_{\mathrm{T}},t_i,\tau_i)$ is the impulse response vector at Rx side for the n_{T}th Tx antenna. The correlation matrix $\mathbf{R}$ is expressed as

$$\mathbf{R}(t_s,\tau_s) = [\![\mathbf{W}(t_i,\tau_i)]\!], \tag{6}$$

where $[\![\cdot]\!]$ operator averages the inner term over time within the s-th WSS region.

By identifying the peaks in the estimated spatial spectrum (averaged over each WSS region), AOA and delay of MPCs are obtained. For each delay bin, MPCs are detected with a peak search along spatial spectrum, one by one accordingly to their amplitudes. Only those peaks separated from the previously detected peak by more than 30 degrees are detected, since the azimuth resolution is approximately 26 degrees [25]. A cutoff threshold of 20 dB below the strongest peak was applied in the peak search, together with a threshold of 6 dB plus noise floor, to ensure that only the effective MPCs are detected since the noise free range of the sounder is 20 dB.

Fig. 1(a) shows an example plot of the estimated P_h in suburban areas, where the power is normalized so that the maximum value of spectrum equals to 0 dB. An azimuth of 0 degree means that the MPC comes from the front of Rx. Fig. 1(b) shows the detected MPCs from the spectrum using the method above. A total of 8 MPCs are detected, and the LOS component is around 240 ns with a AOA of 2 degrees. A visual comparison between Fig. 1(a) and (b) clearly shows that the important MPCs are successfully detected. In this paper, we do not introduce "clusters" for two reasons: (i) We fail to detect a large number of MPCs from the peak search of the Bartlett spectrum, as shown in Fig. 1(b). It is thus difficult to cluster the small number of MPCs with distinct delays and AOAs; (ii) Another strategy is to cluster MPCs over different WSS regions. However, this prevents the dynamic modeling of the cluster evolutions over different WSS regions. Therefore, in this paper we focus on the dynamic modeling of MPCs, instead of clusters, which has sufficient accuracy of analysis (as shown in the later model validation) and reflects reality.

B. MPC Tracking

To capture the dynamic evolutions of MPCs within their lifetimes, a MPC tracking is performed based on MPC distance (MCD) [33]. MCD is a measure to quantify the distance between MPCs. A small value of MCD means that two MPCs are *similar* to each other. This can be used to track MPC and estimate its lifetime.

For two arbitrary MPCs l_1 and l_2, with consecutive indices of WSS windows, the MPCs' information can be expressed as

$$\begin{array}{ll} l_1 \in \mathcal{L}_s & : [\ \overline{a_1(t_s)}, \overline{\tau_1(t_s)}, \overline{\phi_1(t_s)}\ ] \\ l_2 \in \mathcal{L}_{s+1} & : [\ \overline{a_2(t_{s+1})}, \tau_2(t_{s+1}), \overline{\phi_2(t_{s+1})}\ ] \end{array}, \tag{7}$$

where $\overline{(\cdot)}$ means that term $(\cdot)$ is averaged within each WSS region. To improve accuracy, the MCD estimation is revised by introducing a heuristic normalized amplitude factor, as

$$\mathrm{MCD} = \left(\frac{1}{\Delta a_{\max}}\left|\frac{\overline{a_1(t_s)}}{\overline{a_2(t_{s+1})}}\right|\right)\cdot\sqrt{\|\mathrm{MCD}_{\mathrm{AOA}}\|^2 + \mathrm{MCD}_\tau^2}, \tag{8}$$

where vector-valued MCD of AOA is expressed as

$$\mathrm{MCD}_{\mathrm{AOA}} = \frac{1}{2}\cdot\left|\begin{pmatrix}\sin(\overline{\theta_1(t_s)})\cos(\overline{\phi_1(t_s)})\\ \sin(\overline{\theta_1(t_s)})\sin(\overline{\phi_1(t_s)})\\ \cos(\overline{\theta_1(t_s)})\end{pmatrix} - \begin{pmatrix}\sin(\overline{\theta_2(t_{s+1})})\cos(\overline{\phi_2(t_{s+1})})\\ \sin(\overline{\theta_2(t_{s+1})})\sin(\overline{\phi_2(t_{s+1})})\\ \cos(\overline{\theta_2(t_{s+1})})\end{pmatrix}\right|, \tag{9}$$

and $\|\mathrm{MCD}_{\mathrm{AOA}}\|$ represents length of the vector. Elevation angles $\overline{\theta_1(t_s)} = \overline{\theta_2(t_{s+1})} = 90$ degrees. MCD of delay is as

$$\mathrm{MCD}_\tau = \frac{\tau_{\mathrm{std}}}{(\Delta\tau_{\max})^2}\cdot\left|\overline{\tau_1(t_s)} - \overline{\tau_2(t_{s+1})}\right|, \tag{10}$$

where

$$\begin{aligned}\Delta\tau_{\max} &= \max(\overline{\tau_l}) - \min(\overline{\tau_l}) \\ \Delta a_{\max} &= \frac{\max(\overline{a_l})}{\min(\overline{a_l})}\end{aligned}, l \in (\mathcal{L}_s \cup \mathcal{L}_{s+1}), \tag{11}$$

and τ_{std} is a standard deviation of the delays for $l \in (\mathcal{L}_s \cup \mathcal{L}_{s+1})$; $|\cdot|$ denotes absolute value.

A specified threshold ϵ is used to measure the similarity between two MPCs, and to perform tracking. Our tracking algorithm is similar to the spirit of [20], and is based on a two-way-matching, described as follows:

1) Calculating MCD between any MPC within $\mathcal{L}_s$ and any MPC within $\mathcal{L}_{s+1}$, and obtain a MCD matrix $\mathbf{D}$ with dimension $N(t_s)\times N(t_{s+1})$.

2) If conditions

$$\begin{array}{l}\mathbf{D}_{u,v} \le \epsilon \\ u = \arg\min_u(\mathbf{D}_{u\in N(t_s),v}) \\ v = \arg\min_v(\mathbf{D}_{u,v\in N(t_{s+1})})\end{array}, \tag{12}$$

are satisfied, the uth MPC at time t_s and the vth MPC at time t_{s+1} are considered to be the same MPC. To match them, a unique MPC-ID is assigned to them.

3) Examining all other MPCs between time t_s and t_{s+1}, and matching all MPCs according to (12).

4) Calculating MCD between any MPC within $\mathcal{L}_{s+1}$ and any MPC within $\mathcal{L}_{s+2}$, and repeating steps (1) and (2). If the wth MPC at time t_{s+2} is found to match vth MPC at time t_{s+1}, the wth MPC (at time t_{s+2}) inherits the MPC-ID from the vth MPC (at time t_{s+1}); and so forth.

5) Repeating above steps for the times after t_{s+2}, and doing matching in every two consecutive indices of WSS time windows. Assigning MPC-IDs for all MPCs.

Above tracking algorithm starts from $s = 1$. By grouping

This article has been accepted for publication in a future issue of this journal, but has not been fully edited. Content may change prior to final publication. Citation information: DOI 10.1109/TIE.2015.2459376, IEEE Transactions on Industrial Electronics

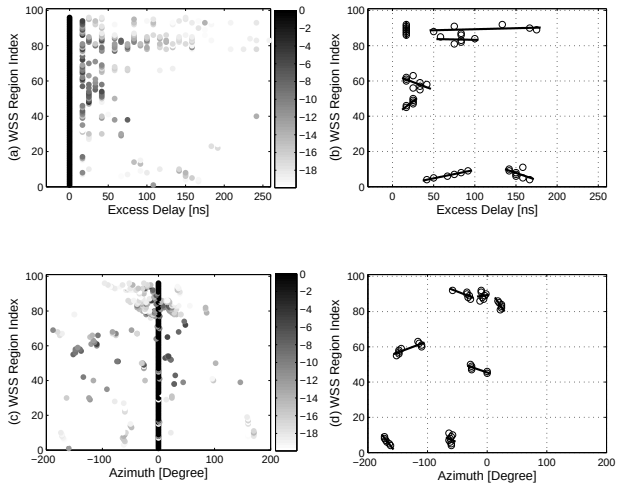

Fig. 2. Example plot in suburban. (a) Detected MPCs (in dB) on delay domain. (b) MPC tracking on delay domain. (c) Detected MPCs (in dB) on azimuth domain. (d) MPC tracking on azimuth domain. In (b) and (d), MPCs with a lifetime of less than 6 WSS windows are not plotted for clarity.

MPCs with identical MPC-IDs, we obtain lifetime and evolutions of each MPC. In this paper, we set $\epsilon = 0.5$, which is validated by visual inspection to have reasonable tracking results, and is also suggested by [20]. Before performing MPC tracking, all the identified MPCs are normalized against the LOS component[6], so that the changes of Tx-Rx distance due to traffics in measurements do not affect model parameters.

Fig. 2 shows an example plot of MPC tracking in suburban. In Fig. 2(b) and (d), results of MPC tracking are marked with linear least-square (LS) regression curves, and the tracking of LOS component (with 0 ns excess delay and 0 degree azimuth) is not presented. Note that for clarity, MPCs with a lifetime of less than 6 WSS windows[7] are not plotted in Fig. 2(b) and (d). However, all the MPCs (with long and short lifetimes) are considered in the dynamic modeling (as detailed in the following section). From Fig. 2 we can see that only those MPCs with similar evolutions on both angular and delay domains are grouped, and our tracking algorithm generally leads to reasonable results. It is also noteworthy that the evolutions of MPCs on angular and delay domains are independent. Furthermore, the track of evolution (i.e., the slope of the LS fit curves) is generally independent of angle and delay. This follows the physical insight that the scatterers are randomly distributed in the dynamic V2V channels.

V. Model Parameters

A. WSS Region

As mentioned in Section III a WSS time window ΔW should be defined so that channel parameters can be statistically modeled. In this paper, we use correlation matrix distance (CMD) [34] to determine the size of WSS region[8], which is useful to evaluate whether the spatial structure of the channel have changed in a significant way. Details of CMD implementation can be found in [8]. The time-variant WSS time window is defined as the maximum period over which CMD remains below a certain threshold $c_{\rm th}$. In this paper, $c_{\rm th}$ is set at 0.2, which was suggested by [35] for V2V channels.

Table I summarizes the estimated ΔW in each environment. It is found that underground parking has the smallest WSS region of 0.95 s, which is mostly due to the tunnel-like structure with the richest scatterers; whereas in suburban with less scatterers, ΔW increases to 1.52 s. In the following, channel parameters are first estimated within each WSS time window ΔW, and then statistically modeled.

B. MPC Lifetime

If one MPC is first observed at the s'th WSS region and is last observed at the s''th WSS region (where $s' \leq s''$), its lifetime T is given by

$$T = \Delta W \cdot \Delta s = \Delta W \cdot (s'' - s' + 1) \ . \tag{13}$$

Instead of modeling T, we model integer Δs so that we can fit data to Poisson distribution for comparison. When modeling Δs, the LOS component is not considered. Fig. 3(a) shows the probability density function (PDF) fit to the measurements. The Poisson, Gamma, Exponential, and truncated Gaussian distributions are plotted for comparison. It is found that the truncated Gaussian distribution fits well to the measurements. Note that due to the poor fit of the Exponential distribution, we do not use Markov process to model the dynamic evolutions. This is because assumption of Markov process implies that MPC' lifetime follows the Exponential distribution [12], [13]. Finally, we model Δs as a truncated Gaussian distribution[9] bounded within $[1, s_{\max}]$, with mean value $\mu_{\Delta s}$ and standard deviation $\sigma_{\Delta s}$, where $s_{\max}$ is the maximum Δs observed in measurements. Parameters of distributions of Δs are estimated using a nonlinear LS regression method and summarized in

[6]The normalization leads to 0 dB power, 0 ns delay, and 0 degree azimuth for LOS component.

[7]The definition of WSS windows is given in Section V.A.

[8]Note that we use the term *WSS regions* not in its mathematical-statistical meaning but to express that the statistics of channel are similar enough compared to statistics of the neighboring channel such that the statistics can be approximately considered to be WSS.

[9]It is found that MPC lifetime is independent of the mean values of MPC delay and AOA within its lifetime.

This article has been accepted for publication in a future issue of this journal, but has not been fully edited. Content may change prior to final publication. Citation information: DOI 10.1109/TIE.2015.2459376, IEEE Transactions on Industrial Electronics

TABLE I
DYNAMIC MODEL PARAMETERS

Parameter	Suburban	Urban	Underground Parking
ΔW [s]	1.52	1.15	0.95
$s_{\max}$	49	48	29
$\mu_{\Delta s}$	1	1	1
$\sigma_{\Delta s}$	10.5	13.0	6.8
p_{11}	1.30	1.81	2.39
p_{12}	7.70	3.05	3.10
p_{21}	1.22	1.48	1.61
p_{22}	9.76	9.12	2.82
σ_ϕ (degree)	46.9	76.2	104.1
$\tau_{a,\mathrm{bp}}$ [ns]	91.67	91.67	66.67
q_1	-0.19	-0.19	-0.30
q_2	-0.008	-0.009	-0.005
q_3	-12.80	-12.93	-13.54
$k_{\tau,(k_\tau>0)}$	9.05	8.09	2.89
$k_{\tau,(k_\tau<0)}$	-5.16	-6.94	-2.53
$k_{\phi,(k_\phi>0)}$	5.19	6.00	17.58
$k_{\phi,(k_\phi<0)}$	-3.46	-7.54	-9.77
$k_{a,(k_a>0,k_\tau>0)}$	0.060	0.060	0.018
$k_{a,(k_a<0,k_\tau>0)}$	-0.045	-0.063	-0.051
$k_{a,(k_a>0,k_\tau<0)}$	0.027	0.042	-0.068
$k_{a,(k_a<0,k_\tau<0)}$	-0.035	-0.041	-0.031
$k_{a,(k_a>0,k_\tau=0)}$	0.009	0.049	0.016
$k_{a,(k_a<0,k_\tau=0)}$	-0.006	-0.004	-0.014
$\tau_{m,\mathrm{bp}}$ [ns]	16	8	8
m_1	3.31	1.20	1.06
m_2	0.53	0.30	0.35

Table I. It is found that the results of suburban and urban are generally close to each other, which means both scenarios lead to similar lifetime characteristics. The underground parking has the smallest $s_{\max}$ and $\sigma_{\Delta s}$. This implies that MPCs in underground parking generally have a short lifetime, which is mainly due to the tunnel-like structure with rich scatterers.

C. Distribution of Number of Newly Observed MPCs

Recall Eq. (3), the total number of MPCs $N(t_{s''})$ at time $t_{s''}$ is determined by the number of new MPCs $N(t_{s''\to s''})$ and the number of old MPCs $N(t_{s'\to s''})$, where $0 < s' \le s''$. Since $N(t_{s'\to s''})$ is determined by $N(t_{s'})$ MPCs at time $t_{s'}$ and their lifetimes, we only need to model the number of new MPCs in each time instant to simulate the dynamic model.

After tracking each MPC in the measurements, we can identify the number of newly observed MPCs in each WSS window. It is found that PDF f_1 of the newly observed MPCs can be well modeled by the Gamma distribution, given by

$$f_1(x; p_{11}, p_{12}) = \frac{x^{p_{11}-1} \cdot \exp\left(-x/p_{12}\right)}{(p_{12}{}^{p_{11}}) \cdot \Gamma(p_{11})}, \qquad (14)$$

where p_{11} and p_{12} are model parameters which can be estimated using the nonlinear LS regression method; $\Gamma(\cdot)$ is the Gamma function. Fig. 3(b) shows the LS fit for the measurements, and results of Poisson distribution (which is widely used to express the probability of a given number of events occurring in a fixed interval of time and/or space) are plotted for comparison. It is found that the Gamma distribution indicates a reasonable fit to the measurements. Parameters p_{11} and p_{12} are summarized in Table I.

D. Joint Distribution of Newly Observed MPCs' Position

It has been widely assumed that the statistics for delay and angle of MPCs are independent in spatial-temporal channel model [36]. In order to test this assumption in V2V channels, scatter plot is shown in Fig. 4(a). It is found that there is no significant correlation between AOA and excess delay. There are MPCs present at nearly all delays and angles, especially for the MPCs with an excess delay less than 400 ns (which have relatively strong power). This is not surprising since in the V2V channels with dynamic and randomly distributed scatterers, there is no reason to expect large or small excess delay for the scatterer from a certain AOA. Based on this evidence, and for the sake of simplicity, we assume that AOAs and excess delays are independent.

We focus on the position distribution of new MPCs, because the position of old MPCs can be modeled by the MPC variation model within lifetime (as reported later), together with initial position when those old MPCs were firstly generated. Finally, the joint PDF of new MPC's position is modeled as

$$f_2(\tau, \phi) = f_{2,\tau}(\tau) \cdot f_{2,\phi}(\phi), \qquad (15)$$

where $f_{2,\tau}(\tau)$ is PDF of MPC excess delay, given by the Gamma PDF

$$f_{2,\tau}(\tau = y \cdot \Delta\tau; p_{21}, p_{22}) = \frac{y^{p_{21}-1} \cdot \exp\left(-y/p_{22}\right)}{(p_{22}{}^{p_{21}}) \cdot \Gamma(p_{21})}, \qquad (16)$$

where parameters p_{21} and p_{22} are estimated using the nonlinear LS regression method; $\Delta\tau$ denotes delay difference between two continuous delay bins. Here we use a transformation $\tau = y \cdot \Delta\tau$ to represent MPC position with delay bin number y (which is integer) instead of delay τ. This enables us to fit the data of $f_{2,\tau}(y)$ to Poisson distribution for comparison; $f_{2,\phi}(\phi)$ is AOA PDF, given by the zero-mean Gaussian PDF

$$f_{2,\phi}(\phi) = \frac{1}{\sigma_\phi \sqrt{2\pi}} \exp\left(-\frac{\phi^2}{2\sigma_\phi^2}\right), \qquad (17)$$

where σ_ϕ is standard deviation. Fig. 3(c) and (d) show that the Gamma and zero-mean Gaussian distributions indicate reasonable fits to $f_{2,\tau}(y)$ and $f_{2,\phi}(\phi)$, respectively. Parameters p_{21}, p_{22}, and σ_ϕ are summarized in Table I, where underground parking leads to the largest σ_ϕ.

E. Initial Power of MPC

Considering the lth MPC that is first observed at the s'th WSS region and is last observed at the s''th WSS region (as in Section V.B), the initial information is given by

$$l: \ [\ \overline{a_l(t_{s'})}, \overline{\tau_l(t_{s'})}, \overline{\phi_l(t_{s'})}\ ]. \qquad (18)$$

Evolution of MPC within its lifetime can thus be modeled as a function of its lifetime index s ($s' \le s \le s''$) and its initial information $[\ \overline{a_l(t_{s'})}, \overline{\tau_l(t_{s'})}, \overline{\phi_l(t_{s'})}\ ]$. In this subsection, we model $\overline{a_l(t_{s'})}$.

Fig. 4(b) shows scatter plot of normalized MPC power against azimuth. It is found that the normalized MPC power is generally independent on MPC azimuth. There are MPCs with high powers present at nearly all angles. Therefore, we model $\overline{a_l(t_{s'})}$ as a function of excess delay. To have a good fit to

This article has been accepted for publication in a future issue of this journal, but has not been fully edited. Content may change prior to final publication. Citation information: DOI 10.1109/TIE.2015.2459376, IEEE Transactions on Industrial Electronics

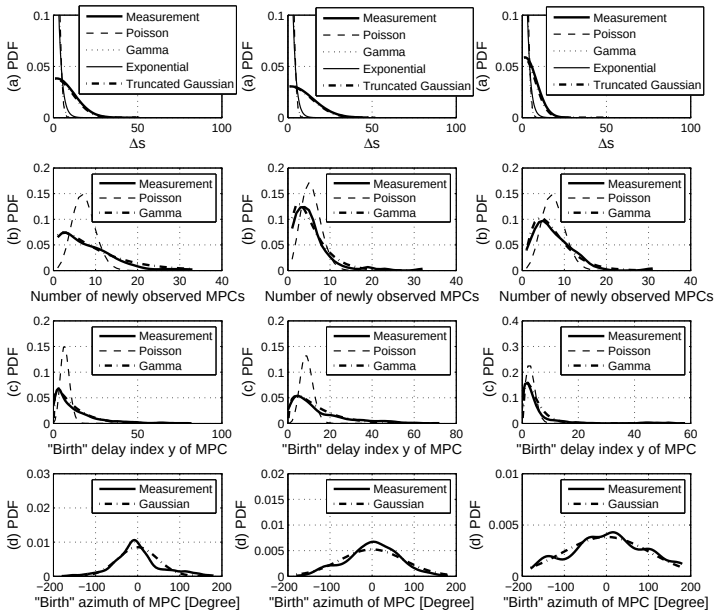

Fig. 3. PDF fits to measurements. Left to right: suburban, urban, and underground parking environments.

the measurements and a small degree of freedom (i.e., a small number of model parameters) in LS fit, $\overline{a_l(t_{s'})}$ is modeled in dB scale and a dual slope model is adopted, expressed as

$$20\log_{10}\left(\overline{a_l(t_{s'})}\right) = \begin{cases} q_1 \cdot \tau[\text{ns}], & 0 \le \tau < \tau_{a,\text{bp}} \\ q_2 \cdot \tau[\text{ns}] + q_3, & \tau_{a,\text{bp}} \le \tau \le 700 \text{ ns} \end{cases}, \tag{19}$$

where $\tau_{a,\text{bp}}$ denotes breakpoint. Parameters q_1, q_2, and q_3 are estimated using the linear LS regression. Note that since we have more samples in measurements with small delays, a direct LS fit over all samples will result in putting a large weight on the samples with small delays. Therefore, we first generate equally-spaced bins of delays with an interval of $\Delta\tau$. Then we calculate the mean power in each equally-spaced delay bin. Finally, we do an LS regression fit using those mean power over equally-spaced delays to get the model. Fig. 4(c) shows LS fit to the measurements in suburban as an example, where it is found that the dual slope model offers a reasonable fit. Results of q_1, q_2, q_3, and τ_{bp} for all three environments are summarized in Table I.

F. MPC Evolution over Consecutive Stationarity Regions

Following the idea of Section V.E, we model variations of amplitude, delay, and azimuth of each MPC within its lifetime but over different WSS regions. Here we distinguish MPCs with *long* and *short* lifetimes, expressed as

$$\Delta s = s'' - s' + 1 : \begin{cases} \ge 6, & \text{long lifetime} \\ < 6, & \text{short lifetime} \end{cases}. \tag{20}$$

The threshold 6 is heuristic, since a visual inspection shows that those MPCs with $\Delta s < 6$ fail to fit to a linear function (which is later used to model MPC evolutions) statistically.

For MPCs with short lifetimes, amplitude, delay, and azimuth are considered to be constant (to avoid poor LS regression fit) within their lifetimes, expressed as

$$\begin{aligned} \overline{a_l(t_s)} &= \overline{a_l(t_{s'})} \\ \overline{\tau_l(t_s)} &= \overline{\tau_l(t_{s'})} \\ \overline{\phi_l(t_s)} &= \overline{\phi_l(t_{s'})} \end{aligned}, \tag{21}$$

where $s' \le s \le s''$. Instead of averaging MPC behaviors in terms of amplitude, delay, and azimuth over their lifetimes, here we use initial information as the model for the MPCs with short lifetimes. This is because when generating MPCs with short lifetimes using the results in Section V.D and V.E, the initial information of MPCs are assigned. MPCs should not change according to our assumption that the MPCs with short lifetimes have *constant* amplitude, delay, and azimuth.

For MPCs with long lifetimes ($\Delta s \ge 6$), the delay and azimuth are modeled using linear polynomial functions, as

$$\begin{aligned} \overline{\tau_l(t_s)} &= \overline{\tau_l(t_{s'})} + k_\tau(s - s' + 1) \\ \overline{\phi_l(t_s)} &= \overline{\phi_l(t_{s'})} + k_\phi(s - s' + 1) \end{aligned}, \tag{22}$$

where parameters k_a, k_τ, and k_ϕ can be estimated using the linear LS regression. Note that the linear polynomial model of $\overline{\tau_l(t_s)}$ and $\overline{\phi_l(t_s)}$ has also been suggested by [12], [13]. In our measurements, k_τ is independent of k_ϕ, and they are both independent of angle and delay, as shown in Fig. 2. This means that within a particular MPC's lifetime, both k_τ and k_ϕ can be positive, or negative, or 0, with equal probability. We thus model evolution of MPCs on angular and delay domains as independent events with equal probability, expressed as

$$\begin{aligned} &\Pr(k_\tau > 0) = \Pr(k_\tau < 0) = \Pr(k_\tau = 0) = 1/3 \\ &\Pr(k_\phi > 0) = \Pr(k_\phi < 0) = \Pr(k_\phi = 0) = 1/3 \end{aligned}, \tag{23}$$

where $\Pr(\cdot)$ denotes probability. For each of above cases, mean values of the estimated k_τ and k_ϕ are recorded, and we use terms $\left(k_{\tau,(k_\tau>0)}, k_{\tau,(k_\tau<0)}, k_{\tau,(k_\tau=0)}\right)$ and $\left(k_{\phi,(k_\phi>0)}, k_{\phi,(k_\phi<0)}, k_{\phi,(k_\phi=0)}\right)$ to represent the values for

This article has been accepted for publication in a future issue of this journal, but has not been fully edited. Content may change prior to final publication. Citation information: DOI 10.1109/TIE.2015.2459376, IEEE Transactions on Industrial Electronics

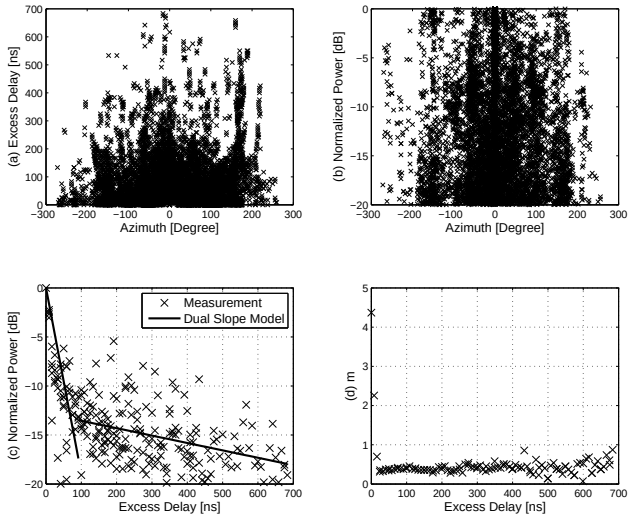

Fig. 4. (a) Scatter plot of azimuth vs excess delay using all the measurements. (b) Scatter plot of power vs azimuth using all the measurements. Powers are normalized so that the power of LOS component equals to 0 dB. (c) Scatter plot and dual slope model of normalized power vs excess delay in suburban. (d) Scatter plot of Nakagami m-parameter vs excess delay in suburban.

above cases, respectively. Results are summarized in Table I. Note that $k_{\tau,(k_\tau=0)} = k_{\phi,(k_\phi=0)} = 0$.

For the model of $\overline{a_l(t_s)}$ within MPC's lifetime, we still use the linear polynomial function to model $\overline{a_l(t_s)}$ and ignore the power variation against the linear fit, which is found to have sufficient accuracy. The model is expressed as

$$\overline{a_l(t_s)} = \overline{a_l(t_{s'})} + k_a(s - s' + 1). \tag{24}$$

As discussed before, amplitude does not depend on AOA, therefore k_a is considered to be independent of k_ϕ. Meanwhile, for different behaviors of k_τ, k_a is found to be either positive or negative[10] with equal probability. Therefore, the evolution of MPC power within lifetime, i.e., k_a, is also modeled as an equal-probability variable, expressed as

$$\begin{aligned}\Pr(k_a>0,k_\tau>0) &= \Pr(k_a<0,k_\tau>0)\\ &= \Pr(k_a>0,k_\tau<0) = \Pr(k_a<0,k_\tau<0)\\ &= \Pr(k_a>0,k_\tau=0) = \Pr(k_a<0,k_\tau=0) = 1/6\end{aligned}. \tag{25}$$

For each of above cases, mean value of the estimated k_a is recorded, and represented as

$$\begin{bmatrix} k_{a,(k_a>0,k_\tau>0)} & k_{a,(k_a<0,k_\tau>0)} & k_{a,(k_a>0,k_\tau<0)} \\ k_{a,(k_a<0,k_\tau<0)} & k_{a,(k_a>0,k_\tau=0)} & k_{a,(k_a<0,k_\tau=0)} \end{bmatrix},$$

which are summarized in Table I. Note that in our measurements, the case $k_a = 0$ does not happen.

Summarizing, the evolutions of MPCs' amplitude, delay, and azimuth within their lifetimes are considered to be events of equal probability. For each event, the variations are modeled as linear functions of their lifetime index. Note that we do not consider those movements of MPCs with more complicated tracks, such as the MPC's delay first increases and then deceases with WSS region index, where a breakpoint model may have better fit. This is because: (i) in our measurements those complicated movements of MPCs rarely occur, or are not distinct; (ii) the automatic tracking algorithm fails to track the complicated movements; and (iii) modeling the complicated tracks would significantly increase model complexity. Therefore, we use the linear polynomial model for simplicity.

G. MPC Fading Behavior

To characterize fading behavior for a certain MPC $[\ \overline{a_l(t_s)}, \overline{\tau_l(t_s)}, \overline{\phi_l(t_s)}\ ]$ within a WSS region, which was extracted from $P_h(t_s, \tau_s, \phi_s)$, we first extract MPCs with the same information of $[\ \overline{\tau_l(t_s)}, \overline{\phi_l(t_s)}\ ]$ from all the other *instantaneous* directional channel impulse response[11] within the s-th WSS region. After removing the mean value of the amplitudes of the extracted instantaneous MPCs within each WSS region, the small-scale fading distribution of $\overline{a_l(t_s)}$ can be characterized within each WSS region.

We use the Akaike Information Criteria (AIC) [37] together with a Kolmogorov-Smirnov (KS) test with a 95% confidence interval to select the small-scale fading distribution, and we consider four widely used distributions: Ricean, Rayleigh, Nakagami, and Weibull distributions. Details of AIC and KS implementations can be found in [38]. Finally, the Nakagami distribution (which has the highest best fit rate of over 85%) is suggested to model the fading distribution of MPCs.

A model of Nakagami shape factor m [38] is proposed to characterize the small-scale fading. Similar to the previous discussion, m is considered to be independent of ϕ. Fig. 4(d) shows the scatter plot of m against excess delay in suburban as an example, where the estimated m's are averaged within each excess delay bin as in Section V.E. It is found that m is very high for small delay bins, and it drops below 0.6 after 16 ns. Similar phenomena are observed in urban and

[10]Note that this phenomenon follows the physical insight of dynamic V2V channels. In the movement of a certain scatterer, e.g., a compact car, when it comes closer to Rx, reflected MPC would have a shorter delay. However, if propagation link between this car and Rx is blocked by other vehicles, a stronger shadowing might be caused when the car comes closer to Rx and a reduced power can be observed.

[11]The instantaneous directional channel impulse responses are derived using $\mathbf{W}$ in Eq. (5), instead of using the WSS region-averaged $\mathbf{R}$ in Eq. (6).

This article has been accepted for publication in a future issue of this journal, but has not been fully edited. Content may change prior to final publication. Citation information: DOI 10.1109/TIE.2015.2459376, IEEE Transactions on Industrial Electronics

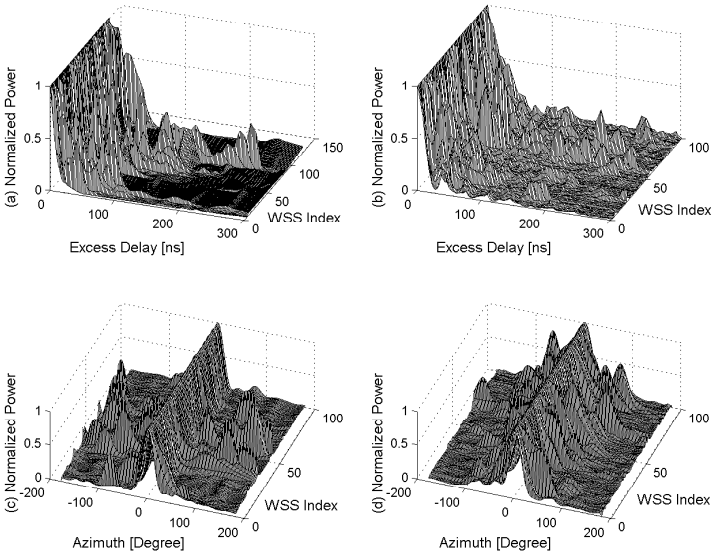

Fig. 5. Comparisons in suburban environment. (a) Measured PDPs. (b) Simulated PDPs. (c) Measured PAPs. (d) Simulated PAPs.

underground parking environments. We thus model m as a piecewise constant model, expressed as

$$m = \begin{cases} m_1, & \tau < \tau_{m,\mathrm{bp}} \\ m_2, & \tau \geq \tau_{m,\mathrm{bp}} \end{cases}, \tag{26}$$

where $\tau_{m,\mathrm{bp}}$ is breakpoint; m_1 and m_2 are mean values of m within the regions before and after breakpoint, respectively. Results are summarized in Table I. It is found that for MPCs with large delays, fading is "worse than Rayleigh" (with $m_2 < 1$). It is also noteworthy that m is generally large in suburban due to the less scatterers, and the underground parking leads to a "close to Rayleigh" fading for the MPCs with small delays.

H. Discussion

Several observations in above results are worth noting:

- The model parameters between suburban and urban are relatively close to each other, which can be found from the values of Δs, p_{21}, p_{22}, q, k_τ, and k_ϕ. We conjecture that this is caused by the similar distribution of scatterers - though urban has richer scatterers, the density does not strongly affect the distribution of scatterers on delay domain and its lifetime and power behaviors, i.e., the model parameters of Eqs. (13), (16), (19), and (22). However, the MPC number (p_{11} and p_{12}) and fading behavior (m) are different in these two scenarios.
- Compared with the *open* environments of suburban and urban, the excess delay of MPC in underground parking is relatively small due to its *close* tunnel-like structure, e.g., the mean $p_{21} \cdot p_{22}$ of Gamma variable in Eq. (16) is the smallest in the underground parking scenario. However, the MPC with small delay has higher power according to Eq. (19), therefore the MPC delay spread is generally large in the underground parking, which is presented later by both measurement and model simulation.
- In suburban and urban, the path length of MPC generally has a larger range compared to the underground parking. Therefore, MPC changes faster on delay domain in its evolution for the suburban and urban scenarios, which is reflected by a larger absolute value of k_τ. However, as the scatterers are closer to Tx and Rx in the tunnel-like underground parking and are generally distributed over all angles, σ_ϕ and the absolute value of k_ϕ are larger in the underground parking scenario.

VI. Model Implementation and Validation

A. Implementation

We summarize model implementation steps as follows:

1) We first set initial MPC number and total number of simulated WSS regions. Lifetime, position, and power of each MPC are initialized using the results in Sections V.B, V.D, and V.E. After initialization, we drop the MPCs with power 20 dB lower than the max. power.

2) In the second WSS region, the old MPCs' lifetimes are first checked to determine whether they are going to be erased or kept. For those remaining MPCs, we categorize them into two groups: MPCs with long and short lifetimes. For the MPCs with short lifetimes, they inherit their initial amplitude, delay, and azimuth in the second WSS region. For the MPCs with long lifetimes, we update amplitude, delay, and azimuth using the results in Section V.F: To determine k_ϕ, we generate a random variable, which could be [1, 2, 3] with equal probability. Each value corresponds to one possible event of k_ϕ in (23). We thus update azimuth of MPC using obtained k_ϕ and the model of (22). To determine k_a and k_τ, we generate a random variable, which could be [1, 2, 3, 4, 5, 6] with equal probability. Each value corresponds to one possible event of k_a and k_τ in (25). We thus update amplitude and delay of MPC using obtained k_a and k_τ and the model of (24).

3) Then we generate number N_2 of new MPCs in the second WSS region, using the results in Section V.C. If $N_2 > 0$, we initialize lifetime, position, and power of the N_2 new MPCs.

This article has been accepted for publication in a future issue of this journal, but has not been fully edited. Content may change prior to final publication. Citation information: DOI 10.1109/TIE.2015.2459376, IEEE Transactions on Industrial Electronics

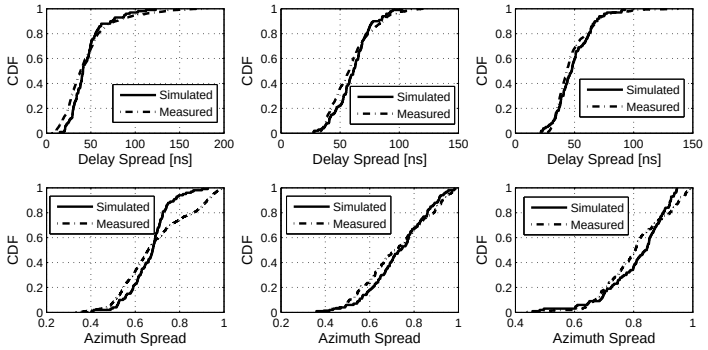

Fig. 6. Comparisons of $\tau_{\rm rms}$ and $\phi_{\rm rms}$ between simulated and measured channels. Left to right: suburban, urban, and underground parking. $\phi_{\rm rms} = 1$ indicates that signal arrives at Rx uniformly spread over all directions, whereas $\phi_{\rm rms} = 0$ implies that signal arrives from a single direction.

Finally, we drop the MPCs with power 20 dB lower than the max. power.

4) By repeating steps 2 and 3, we can simulate channels in consecutive WSS regions using the results in Table I.

Above simulated impulse responses are normalized against LOS component. Tx-Rx distance can be set as required to reflect Tx and Rx movements, and a model of LOS component can refer to two-ray model [39]. In each WSS region, the small-scale fading can be simulated by generating $N_{\rm ss}$ Nakagami-distributed variables using Section V.G. The mean amplitude of Nakagami-distributed variables is set to be the generated amplitude using steps above.

B. Validation

With the proposed model, we can generate the angular-delay spectrum $\tilde{P}_h(t_s, \tau, \phi)$ for the s-th WSS region. For comparison, the generated impulse response is integrated over azimuth and delay, respectively, to get power delay profile (PDP) $\mathcal{P}$ and power azimuth profile (PAP) $\mathcal{A}$, given by

$$\begin{aligned} \mathcal{P}(t_s, \tau) &= \sum_{\phi} \tilde{P}_h(t_s, \tau, \phi) \\ \mathcal{A}(t_s, \phi) &= \sum_{\tau} \tilde{P}_h(t_s, \tau, \phi) \end{aligned} . \tag{27}$$

To simulate PDPs, the generated channel impulse responses are filtered using a sinc filter (to have the same bandwidth as in the measurements). The simulated PAPs are filtered using the Bartlett beamformer as in Section IV.A to estimate the corresponding spatial spectrum.

We generate impulse responses for 100 consecutive WSS regions in suburban. Initial MPC number is set to be 7 according to measurements. Fig. 5 shows the measured and simulated PDPs and PAPs in suburban. Since the comparison is performed between statistical realizations, the agreement can be evaluated only qualitatively. It is observed that the measured and simulated PDPs and PAPs do agree in that sense. Regarding the complexity of the model, we found that the total running time of generating impulse responses for one WSS region is around 0.0045 s (in Matlab 2012, with 4GB RAM computer), which shows that the model has very low complexity of simulation. The most time-consuming part is to generate a random variable to determine MPC evolution behavior (as in Section V.F), which takes 38% of the total running time. However, it is found that calculating the channel transfer functions from the set of plane waves takes longer time (around 0.05 s for each snapshot) compared with channel generation, and a method in [40] can be used to reduce the running time of channel transfer function calculations.

To further validate the model, two second-order statistics, the root-mean-square (RMS) delay spread $\tau_{\rm rms}$ and azimuth direction spread $\phi_{\rm rms}$ [41], are used. Fig. 6 shows the cumulative distribution function (CDF) comparisons of $\tau_{\rm rms}$ and $\phi_{\rm rms}$ between simulated and measured channels, where the simulation is fairly close to the measurements. We use a two-sample t-test with the significant level of 5% [42] to evaluate the agreement of simulation with measurements in Fig. 6, and it is found that the t-test never rejects the null hypothesis in all cases, which validates the model. Note that there are some differences between the simulated and measured results of $\phi_{\rm rms}$ in suburban, where the simulated CDFs tend to be slightly narrower than the measured ones. A possible explanation is that the simulated CDFs may be partially affected by the model error of σ_ϕ in Eq. (17). Again, we find the overall performance of the model satisfactory accordingly to the t-test.

VII. Conclusion

In this paper, a dynamic wideband directional model is proposed for time-variant V2V channels. The model is developed in V2V suburban, urban, and underground parking environments based on a large set of measurements at 5.3 GHz. By incorporating both angular and delay domain properties as well as dynamic behaviors of MPC's evolutions, the model is capable of handling time-variant V2V scenarios with dynamic scatterers. The PDFs of the number of MPCs, lifetime, and position are fitted to the best theoretical distributions. A delay-based model is proposed to describe MPC's power, and a linear polynomial function is used to model the variations of MPC's behaviors within its lifetime. Fading behavior of MPC is characterized by the Nakagami distribution and variation of the m-parameter over delay is modeled. The model implementation is detailed and, finally, the model is validated by comparing key statistics of simulations with measurements. The proposed model shows insight into the dynamic behaviors of MPCs in V2V environments, and provides a realistic simulation model for performance evaluation of wireless vehicular networks.

VIII. Acknowledgments

The authors would like to thank P. Vainikainen, J. Koivunen, and M. Olkkonen for their contributions in the measurements. Olivier Renaudin acknowledges the financial support of the Belgian Fonds Spécial de la Recherche Scientifique (FRS).

References

[1] R. He, O. Renaudin, V.-M. Kolmonen, K. Haneda, Z. Zhong, B. Ai, and C. Oestges, "Statistical characterization of dynamic multi-path components for vehicle-to-vehicle radio channels," in *Proc. IEEE Veh. Technol. Conf. (VTC'15)*, 2015, pp. 1–6.

[2] P. Bello, "Characterization of randomly time-variant linear channels," *IEEE Trans. Commun. Syst.*, vol. 11, no. 4, pp. 360–393, 1963.

[3] N. Akhtar, S. Coleri Ergen, and O. Ozkasap, "Vehicle mobility and communication channel models for realistic and efficient highway VANET simulation," *IEEE Trans. Veh. Technol.*, vol. 64, no. 1, pp. 248–262, 2015.

[4] L. Bernadó, T. Zemen, F. Tufvesson, A. F. Molisch, and C. F. Mecklenbrauker, "Time-and frequency-varying-factor of non-stationary vehicular channels for safety-relevant scenarios," *IEEE Trans. Intell. Transp. Syst.*, vol. 16, no. 2, pp. 1007–1017, 2015.

[5] S. Zhu, T. S. Ghazaany, S. M. Jones, R. Abd-Alhameed, J. M. Noras, T. Van Buren, J. Wilson, T. Suggett, and S. Marker, "Probability distribution of rician K-factor in urban, suburban and rural areas using real-world captured data," *IEEE Trans. Antennas Propag.*, vol. 62, no. 7, pp. 3835–3839, 2014.

[6] T. Abbas, L. Bernado, A. Thiel, C. Mecklenbrauker, and F. Tufvesson, "Radio channel properties for vehicular communication: Merging lanes versus urban intersections," *IEEE Veh. Technol. Mag.*, vol. 8, no. 4, pp. 27–34, 2013.

[7] D. W. Matolak, "Channel modeling for vehicle-to-vehicle communications," *IEEE Commun. Mag.*, vol. 46, no. 5, pp. 76–83, 2008.

[8] O. Renaudin, V.-M. Kolmonen, P. Vainikainen, and C. Oestges, "Non-stationary narrowband MIMO inter-vehicle channel characterization in the 5-GHz band," *IEEE Trans. Veh. Technol.*, vol. 59, no. 4, pp. 2007–2015, 2010.

[9] L. Bernadó, T. Zemen, A. Paier, and J. Karedal, "Complexity reduction for vehicular channel estimation using the filter divergence measure," in *Proc. IEEE Asilomar Conf. Signals Syst. Comput. (ASSC'10)*, 2010, pp. 141–145.

[10] O. Renaudin, V.-M. Kolmonen, P. Vainikainen, and C. Oestges, "Wide-band measurement-based modeling of inter-vehicle channels in the 5-GHz band," *IEEE Trans. Veh. Technol.*, vol. 62, no. 8, pp. 3531–3540, 2013.

[11] J. Karedal, F. Tufvesson, N. Czink, A. Paier, C. Dumard, T. Zemen, C. F. Mecklenbrauker, and A. F. Molisch, "A geometry-based stochastic MIMO model for vehicle-to-vehicle communications," *IEEE Trans. Wireless Commun.*, vol. 8, no. 7, pp. 3646–3657, 2009.

[12] Y. Chen and V. K. Dubey, "Dynamic simulation model of indoor wideband directional channels," *IEEE Trans. Veh. Technol.*, vol. 55, no. 2, pp. 417–430, 2006.

[13] C.-C. Chong, C.-M. Tan, D. I. Laurenson, S. McLaughlin, M. A. Beach, and A. R. Nix, "A novel wideband dynamic directional indoor channel model based on a Markov process," *IEEE Trans. Wireless Commun.*, vol. 4, no. 4, pp. 1539–1552, 2005.

[14] J. Ø. Nielsen, V. Afanassiev, and J. B. Andersen, "A dynamic model of the indoor channel," *Wireless Person. Commun.*, vol. 19, no. 2, pp. 91–120, 2001.

[15] R. J. Piechocki, J. P. McGeehan, and G. V. Tsoulos, "A new stochastic spatio-temporal propagation model (SSTPM) for mobile communications with antenna arrays," *IEEE Trans. Commun.*, vol. 49, no. 5, pp. 855–862, 2001.

[16] W. Wang, T. Jost, U. Fiebig, and W. Koch, "Time-variant channel modeling with application to mobile radio based positioning," in *Proc. IEEE Global Telecommun. Conf. (GLOBECOM'12)*, 2012, pp. 5038–5043.

[17] M. L. Jakobsen, T. Pedersen, and B. H. Fleury, "Analysis of stochastic radio channels with temporal birth-death dynamics: A marked spatial point process perspective," *IEEE Trans. Antennas Propag.*, vol. 62, no. 7, pp. 3761–3775, 2014.

[18] M. L. Jakobsen, T. Pedersen, and B. Fleury, "Simulation of birth-death dynamics in time-variant stochastic radio channels," in *Proc. Int. Zurich Seminar Commun.*, 2014, pp. 124–127.

[19] B.-F. Wu and C.-L. Jen, "Particle filter based radio localization for mobile robots in the environments with low-density WLAN APs," *IEEE Trans. Ind. Electron.*, vol. 61, no. 12, pp. 6860–6870, 2014.

[20] N. Czink, C. Mecklenbrauker, and G. Del Galdo, "A novel automatic cluster tracking algorithm," in *Proc. IEEE Int. Symp. Person. Indoor. Mobile. Radio. Commun. (PIMRC'06)*, 2006, pp. 1–5.

[21] C.-I. Chen and Y.-C. Chen, "Comparative study of harmonic and inter-harmonic estimation methods for stationary and time-varying signals," *IEEE Trans. Ind. Electron.*, vol. 61, no. 1, pp. 397–404, 2014.

[22] C.-I. Chen and G. W. Chang, "An efficient prony-based solution procedure for tracking of power system voltage variations," *IEEE Trans. Ind. Electron.*, vol. 60, no. 7, pp. 2681–2688, 2013.

[23] S. K. Jain, S. Singh, and J. Singh, "An adaptive time-efficient technique for harmonic estimation of nonstationary signals," *IEEE Trans. Ind. Electron.*, vol. 60, no. 8, pp. 3295–3303, 2013.

[24] O. Renaudin, "Experimental channel characterization for vehicle-to-vehicle communication systems," Ph.D. dissertation, Université Catholique de Louvain, Louvain-la-Neuve, Belgium, Aug. 2013.

[25] V. Kolmonen, J. Kivinen, L. Vuokko, and P. Vainikainen, "5.3-GHz MIMO radio channel sounder," *IEEE Trans. Instrum. Meas.*, vol. 55, no. 4, pp. 1263–1269, 2006.

[26] J. Choi, N.-G. Kang, Y.-S. Sung, J.-S. Kang, and S.-C. Kim, "Frequency-dependent UWB channel characteristics in office environments," *IEEE Trans. Veh. Technol.*, vol. 58, no. 7, pp. 3102–3111, 2009.

[27] P. Pajusco and P. Pagani, "Frequency dependence of the UWB indoor propagation channel," in *Proc. IEEE Eur. Conf. Antennas Propag. (EuCAP'07)*, 2007, pp. 1–7.

[28] J. Meinilä, P. Kyösti, T. Jämsä, and L. Hentilä, "WINNER II channel models," *Radio Technologies and Concepts for IMT-Advanced*, pp. 39–92, 2009.

[29] L. Liu, C. Oestges, J. Poutanen, K. Haneda, P. Vainikainen, F. Quitin, F. Tufvesson, and P. Doncker, "The COST 2100 MIMO channel model," *IEEE Wireless Commun.*, vol. 19, no. 6, pp. 92–99, 2012.

[30] H. Krim and M. Viberg, "Two decades of array signal processing research: the parametric approach," *IEEE Signal Processing Mag.*, vol. 13, no. 4, pp. 67–94, 1996.

[31] R. Sarkis, "Antenna arrays for direction of arrival estimation and imaging: from mutual coupling analysis to real-world design," Ph.D. dissertation, Universite Catholique de Louvain, 2011.

[32] Y. Ma, Y. Yang, Z. He, K. Yang, C. Sun, and Y. Wang, "Theoretical and practical solutions for high-order superdirectivity of circular sensor arrays," *IEEE Trans. Ind. Electron.*, vol. 60, no. 1, pp. 203–209, 2013.

[33] M. Steinbauer, H. Ozcelik, H. Hofstetter, C. F. Mecklenbrauker, and E. Bonek, "How to quantify multipath separation," *IEICE Trans. Electron.*, vol. 85, no. 3, pp. 552–557, 2002.

[34] M. Herdin, "Non-stationary indoor MIMO radio channels," Ph.D. dissertation, Technische Universität Wien, Vienna, Austria, Aug. 2004.

[35] R. He, O. Renaudin, V.-M. Kolmonen, K. Haneda, Z. Zhong, B. Ai, and C. Oestges, "Characterization of quasi-stationarity regions for vehicle-to-vehicle radio channels," *IEEE Trans. Antennas Propag.*, vol. 63, no. 5, pp. 2237–2251, 2015.

[36] Q. H. Spencer, B. D. Jeffs, M. A. Jensen, and A. L. Swindlehurst, "Modeling the statistical time and angle of arrival characteristics of an indoor multipath channel," *IEEE J. Sel. Areas Commun.*, vol. 18, no. 3, pp. 347–360, 2000.

[37] K. P. Burnham and D. R. Anderson, *Model selection and multi-model inference: a practical information-theoretic approach*. Springer, 2002.

[38] U. G. Schuster and H. Bolcskei, "Ultrawideband channel modeling on the basis of information-theoretic criteria," *IEEE Trans. Wireless Commun.*, vol. 6, no. 7, pp. 2464–2475, 2007.

[39] J. Karedal, N. Czink, A. Paier, F. Tufvesson, and A. F. Molisch, "Path loss modeling for vehicle-to-vehicle communications," *IEEE Trans. Veh. Technol.*, vol. 60, no. 1, pp. 323–328, 2011.

[40] N. Czink, F. Kaltenberger, Y. Zhou, L. Bernadó, T. Zemen, and X. Yin, "Low-complexity geometry-based modeling of diffuse scattering," in *Proc. IEEE Eur. Conf. Antennas Propag. (EuCAP'10)*, 2010, pp. 1–4.

[41] T. Abbas, J. Karedal, F. Tufvesson, A. Paier, L. Bernadó, and A. F. Molisch, "Directional analysis of vehicle-to-vehicle propagation channels," in *Proc. IEEE Veh. Technol. Conf. (VTC'11)*, 2011, pp. 1–5.

[42] K. Haneda, J. Poutanen, V.-M. Kolmonen, L. Liu, F. Tufvesson, P. Vainikainen, and C. Oestges, "Validation of the COST2100 channel model in indoor environments," in *Proc. Newcom++/COST2100 Joint Workshop*, 2011, pp. 1–6.

This article has been accepted for publication in a future issue of this journal, but has not been fully edited. Content may change prior to final publication. Citation information: DOI 10.1109/TIE.2015.2459376, IEEE Transactions on Industrial Electronics

Ruisi He (S'11-M'13) received the B.E. and Ph.D. degrees from Beijing Jiaotong University, Beijing, China, in 2009 and 2015, respectively. He is currently an Associate Professor with the State Key Laboratory of Rail Traffic Control and Safety, Beijing Jiaotong University, Beijing, China. From 2010 to 2014, He has been a Visiting Scholar in Universidad Politécnica de Madrid, Spain, University of Southern California, USA, and Université Catholique de Louvain, Belgium. His current research interests include radio wave propagation, vehicular communications, LTE-Railways, and 5G communications.

Dr. He serves as the Early Career Representative of Commission C, International Union of Radio Science (URSI), as a TPC chair of "Antenna and wave propagation" for APEMC 2015, and as a TPC member for many conferences. He received the URSI Young Scientist Award in 2015.

Olivier Renaudin received the Electrical Engineering degrees from the Ecole Nationale Supérieure d'Electronique, Informatique et Radiocommunications de Bordeaux (ENSEIRB) and the Université Bordeaux 1, Bordeaux, France, respectively, in 2006. He then joined the Université catholique de Louvain (UCLouvain), Louvain-la-Neuve, Belgium, where he received the PhD degree in 2013. His doctoral research dealt with the experimental characterization of the radio propagation channel for vehicle-to-vehicle communication systems. He was involved in the European COST 2100 Action "Pervasive Mobile & Ambient Wireless Communications".

Since May 2014, he works as a postdoctoral researcher in the Wireless Devices and Systems Group at University of Southern California, Los Angeles, USA. His current research interests include channel sounding, characterization and modeling as well as high-resolution parameter extraction techniques.

Veli-Matti Kolmonen received the M.Sc. degree in technology from Helsinki University of Technology (TKK), Espoo, Finland, in 2004 and the D.Sc. degree in technology from Aalto University, Espoo, Finland in 2010. From 2003 to 2012, he was with the Department of Radio Science and Engineering, Aalto University, first as a Research Assistant, then as a Researcher, and finally as a Postdoctoral Researcher. He was with Philips Medical Systems MR Finland. Currently he is with Nokia Technologies, Finland.

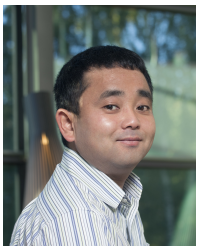

Katsuyuki Haneda (M'08) received the Doctor of Engineering from the Tokyo Institute of Technology, Tokyo, Japan, in 2007. Dr. Haneda is presently an assistant professor in the Aalto University School of Electrical Engineering. Dr. Haneda was the recipient of the best paper award of the IEEE 77th Vehicular Technology Conference, and of the best propagation paper award in the 7th European Conference on Antennas and Propagation. Dr. Haneda has been serving as an associate editor for the IEEE Transactions on Antennas and Propagation since 2012 and as an editor for the IEEE Transactions on Wireless Communications since 2013. He also served as a co-chair of the topical working group on indoor environment and has been an active member of the European COST Action IC1004. His current research activity focuses on high-frequency radios, wireless for medical and post-disaster scenarios, radio wave propagation prediction, and in-band full-duplex radio technologies.

Zhangdui Zhong received the B.E. and M.S. degrees from Beijing Jiaotong University, Beijing, China, in 1983 and 1988, respectively. He is a Professor with Beijing Jiaotong University, Beijing, China. He is currently a Director of the School of Computer and Information Technology and a Chief Scientist of State Key Laboratory of Rail Traffic Control and Safety, Beijing Jiaotong University. He is also a Director of the Innovative Research Team of Ministry of Education, Beijing, and a Chief Scientist of Ministry of Railways, Beijing. His interests include wireless communications for railways, control theory and techniques for railways, and GSM-R systems. He has authored or coauthored seven books, five invention patents, and over 200 scientific research papers in his research area. He received the MaoYiSheng Scientific Award of China, ZhanTianYou Railway Honorary Award of China, and Top 10 Science/Technology Achievements Award of Chinese Universities.

Bo Ai (M'00-SM'10) received his Ph.D. from Xidian University in 2004. He is a professor and Ph.D. advisor at Beijing Jiaotong University. He is the deputy director of State Key Lab of Rail Traffic Control and Safety in China. He has authored /co-authored six books and more than 220 papers. His research interests are focused on rail traffic mobile communications and channel modeling. He is an associate editor of IEEE TRANSACTIONS ON CONSUMER ELECTRONICS and an Editorial Committee Member of the Wireless Personal Communications journal. He has received many awards such as the Qiushi Outstanding Youth Award by HongKong Qiushi Foundation, the New Century Talents by the Chinese Ministry of Education, the Zhan Tianyou Railway Science and Technology Award by the Chinese Ministry of Railways, and the Science and Technology New Star by the Beijing Municipal Science and Technology Commission. He is IEEE Senior member and IET Fellow.

Claude Oestges (M'05-SM'12) received the M.Sc. and Ph.D. degrees in Electrical Engineering from the Université catholique de Louvain (UCL), Belgium, respectively in 1996 and 2000. In January 2001, he joined as a post-doctoral scholar the Smart Antennas Research Group, Stanford University, USA. From January 2002 to September 2005, he was associated with the Microwave Laboratory UCL as a post-doctoral fellow of the Belgian Fonds de la Recherche Scientifique. Claude Oestges is presently Professor with the Electrical Engineering Department, UCL. He also currently serves as an Associate Editor for the IEEE Transactions on Antennas and Propagation and the IEEE Transactions on Vehicular Technology. He is the author or co-author of three books and more than 200 journal papers and conference communications, and was the recipient of the 1999-2000 IET Marconi Premium Award and of the IEEE Vehicular Technology Society Neal Shepherd Award in 2004 and 2012.